JACS
JOURNAL OF THE AMERICAN CHEMICAL SOCIETY

Communication

pubs.acs.org/JACS

A Structurally Characterized Nonheme Cobalt–Hydroperoxo Complex Derived from Its Superoxo Intermediate via Hydrogen Atom Abstraction

Chun-Chieh Wang,[†,‡] Hao-Ching Chang,[†] Yei-Chen Lai,[‡] Huayi Fang,[§] Chieh-Chin Li,[‡] Hung-Kai Hsu,[†] Zong-Yan Li,[†] Tien-Sung Lin,[⊥] Ting-Shen Kuo,[†] Frank Neese,[§] Shengfa Ye,*[,§] Yun-Wei Chiang,*[,‡] Ming-Li Tsai,*[,#] Wen-Feng Liaw,*[,‡] and Way-Zen Lee*[,†]

[†]Department of Chemistry and Instrumentation Center, National Taiwan Normal University, Taipei 11677, Taiwan

[‡]Department of Chemistry, National Tsing Hua University, Hsinchu 30013, Taiwan

[§]Max-Planck Institut für Chemische Energiekonversion, Mülheim an der Ruhr D-45470, Germany

[⊥]Department of Chemistry, Washington University, St. Louis, Missouri 63130, United States

[#]Department of Chemistry, National Sun Yat-sen University, Kaohsiung 80424, Taiwan

Supporting Information

ABSTRACT: Bubbling O_2 into a THF solution of Co^{II}(BDPP) (**1**) at −90 °C generates an O_2 adduct, Co(BDPP)(O_2) (**3**). The resonance Raman and EPR investigations reveal that **3** contains a low spin cobalt(III) ion bound to a superoxo ligand. Significantly, at −90 °C, **3** can react with 2,2,6,6-tetramethyl-1-hydroxypiperidine (TEMPOH) to form a structurally characterized cobalt(III)-hydroperoxo complex, Co^{III}(BDPP)(OOH) (**4**) and TEMPO•. Our findings show that cobalt(III)-superoxo species are capable of performing hydrogen atom abstraction processes. Such a stepwise O_2-activating process helps to rationalize cobalt-catalyzed aerobic oxidations and sheds light on the possible mechanism of action for Co-bleomycin.

Transformation of superoxo to peroxo is a critical step in the catalytic cycles of a range of O_2-activating iron enzymes. For instance, the iron-superoxo intermediates of isopenicillin-*N*-synthase (IPNS)[1] and myo-inositol oxygenase (MIOX)[2] undertake hydrogen atom abstraction (HAA), leading to formation of hydroperoxo species. In the case of homoprotocatechuate 2,3-dioxygenase (Fe-HPCD), the superoxo species is shown to attack an electron-deficient carbon to yield an alkylperoxo intermediate.[3] Unexpectedly, parallel investigations on the Co-reconstituted HPCD (Co-HPCD) demonstrated that its reactivity is even superior to that of Fe-HPCD under O_2-saturating conditions,[4] implying that cobalt, a nonphysiological metal cofactor, may play a similar role as iron in O_2 reduction. Although a series of heme and nonheme cobalt-superoxo complexes have been synthesized and spectroscopically and structurally characterized since the 1970s,[5,6] their reactivity toward organic substrates is barely discussed. Recently, aerobic oxidation of *p*-hydroquinone catalyzed by a salophen-based cobalt complex was reported,[7] for which the density functional theory (DFT) calculations suggested that the cobalt-superoxo species can exhibit HAA reactivity and convert to the corresponding hydroperoxo complex, akin to the iron congeners. Note that Fe-/Co-OOH species, presumably generated by O_2 activation via the superoxo intermediate, have long been postulated to be responsible for DNA cleavage in the mechanism of cancer treatment by bleomycin, a broad-spectrum antitumor agent.[8−10] On the basis of our previous investigation of a nonheme iron-superoxo complex produced from its iron(II) precursor, Fe(BDPP)[11] (H_2BDPP = 2,6-bis((2-(*S*)-diphenylhydroxylmethyl-1-pyrrolidinyl)methyl)-pyridine), we herein present a structurally characterized nonheme cobalt(III)-hydroperoxo complex derived from its superoxo intermediate via HAA (Scheme 1, **3** → **4**).

A purple cobalt(II) complex, Co(BDPP) (**1**), was synthesized from the reaction of $CoCl_2$ with the deprotonated $BDPP^{2-}$ ligand in THF-CH_3CN mixed solvent and structurally characterized by X-ray crystallography (Figure 1A). Similar to Fe(BDPP), **1** features a distorted square pyramidal geometry (τ_5 = 0.58, cf. τ_5 = 0.48 for Fe(BDPP)) in an N_3O_2

Scheme 1. Different Reaction Routes for the Formation of Co^{III}(BDPP)(OOH) (4)

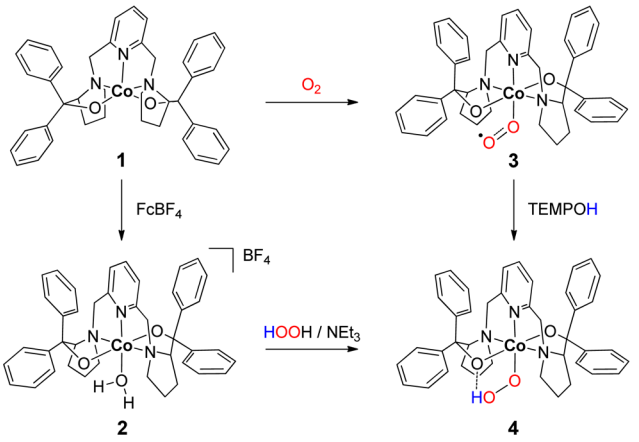

Received: August 18, 2016
Published: October 11, 2016

DOI: 10.1021/jacs.6b08642
J. Am. Chem. Soc. 2016, 138, 14186−14189

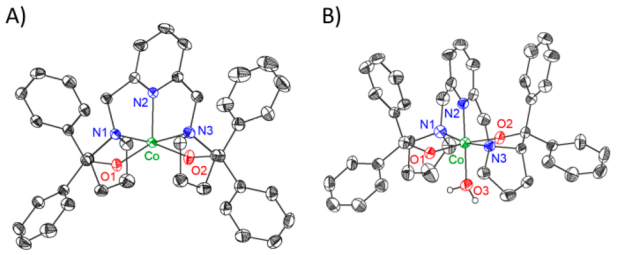

Figure 1. ORTEP of (A) **1** and (B) **2** with ellipsoids set at 50% probability. Anion and hydrogen atoms except water molecule are omitted for clarity.

coordination environment, providing a substrate binding site on the metal center. The selected bond lengths of **1** are listed in Table 1. In contrast to highly air-sensitive Fe(BDPP), **1** is quite

Table 1. Selected Bond Lengths of 1, 2, and 4

	1	2	4
Co–N1 (Å)	2.229(3)	1.991(4)	2.000(2)
Co–N2 (Å)	2.052(5)	1.837(4)	1.875(2)
Co–N3 (Å)	2.229(3)	1.990(3)	1.999(2)
Co–O1 (Å)	1.913(3)	1.881(3)	1.8819(19)
Co–O2 (Å)	1.913(3)	1.862(3)	1.9203(19)
Co–O3 (Å)		1.966(4)	1.9005(19)
O3–O4 (Å)			1.497(3)

stable under air. Cyclic voltammetry of **1** in CH_2Cl_2 shows one reversible redox wave at −476 mV ($E_{1/2}$ vs Fc^+/Fc); chemical oxidation of **1** by $FcBF_4$ in acetone affords a six-coordinate cobalt(III) complex, $[Co(BDPP)(H_2O)](BF_4)$ (**2**, Figure 1B), with a shrunk first coordination sphere (Table 1). The fitting of the SQUID data (Figures S10, S11) show that **1** contains a high-spin Co^{II} center (S = 3/2) with a $g_{iso} \sim 2.48$ and a large axial zero-field splitting (ZFS) parameter ($|D|$ = 15.4 cm^{-1}). The EPR spectrum of a frozen CH_2Cl_2 solution of **1** exhibits a pseudoaxial pattern with effective g values at 4.287 ($g_{eff,\perp}$) and 1.994 ($g_{eff,\parallel}$, $A_\parallel$ = 310 MHz, Figure 2A). The simulation gives

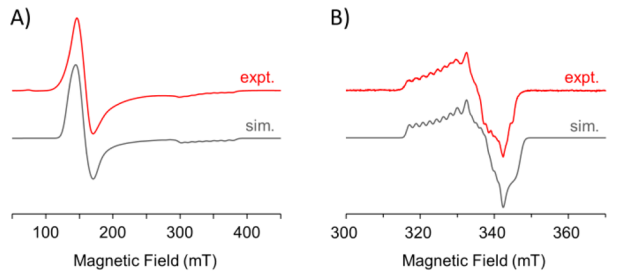

Figure 2. X-band EPR spectra (red) of (A) **1** at 4 K and (B) **3** at 77 K in CH_2Cl_2. Simulations (gray) were performed by EasySpin.

the intrinsic $g_\perp$ at 2.253 and $g_\parallel$ at 1.991 with $D = -13 \pm 3$ cm^{-1} and the rhombicity parameter $|E/D| = 0.04 \pm 0.005$ (Figure 2A), consistent with the SQUID measurements. Considering the large D value, the transitions between the two Kramers' doublets ($m_s = \pm 3/2, \pm 1/2$) are impossible with the X-band frequency. The g values observed arise from the $m_s = \pm 1/2$ transition and shifted by large g anisotropy. The analogous spin Hamiltonian parameters were found for the recently characterized cobalt(II) complexes as well.[6,7,12,13]

Monitored by UV–vis spectroscopy, no reaction of **1** with O_2 in THF is detected at room temperature (Figure S7). On the other hand, an O_2 adduct, $Co(BDPP)(O_2)$ (**3**), forms below −70 °C as indicated by the color of the reaction solution varying from pale purple to marigold with the new absorption bands at 485 and 580 nm (Figure S3). Furthermore, at an even lower temperature, −90 °C, vigorously bubbling N_2 through the marigold solution does not cause discernible changes in the electronic absorption spectrum. The UV–vis absorption, however, converts back to that of **1** upon rapidly raising the temperature of the solution. As elaborated by an earlier systematic study on a series of cobalt complexes, the O_2 addition is an equilibrium with ΔS around −50 ± 10 cal/mol·K and ΔH about −11 ± 4 kcal/mol.[5a] Therefore, at ambient temperature the $-T\Delta S$ factor substantially outweighs the stabilizing enthalpy ΔH contribution; thus, the O_2 coordination is thermodynamically unfavorable. In comparison with **1**, the O_2 binding to Fe(BDPP) is reversible at −80 °C.[10] Different O_2 affinity at ambient temperature is also observed for Co- and Fe-HPCD.[4]

The resonance Raman (rRaman) and EPR measurements evidence that **3** is a cobalt(III)-superoxo complex. The rRaman spectra of **3** (λ_{ex} at 457 nm, Figure S15) show an O–O stretching vibration at 1135 cm^{-1}, which shifts to 1070 cm^{-1} ($\Delta\nu$ = −65 cm^{-1}) upon ^{18}O substitution. Both values fall within the typical range of O–O stretching frequencies found for mononuclear end-on superoxo complexes (Table 2). The

Table 2. Raman Data for Superoxo and Hydroperoxo Species

complex[a]	$\nu(^{16}O-^{16}O)$, cm^{-1}	$\nu(^{18}O-^{18}O)$, cm^{-1}	reference
3	1135	1070	this work
$Fe^{III}(BDPP)(O_2)$	1125	1062	11
$[Fe^{III}(TAML)(\eta^2\text{-}O_2)]^{2-}$	1260	1183	19
$Fe^{III}(Tp^{Me2})(L^{Ph})(O_2)$	1168[b]	1090	6
$Co^{III}(Tp^{Me2})(L^{Ph})(O_2)$	1150	1090	6
Co^{III}(salen)(py)(O_2)	1144	1082	20
4	795	748	this work
$[Fe^{III}(14\text{-}TMC)(OOH)]^{2+}$	868	820	21
$Fe^{III}(Tp^{Me2})(L^{Ph})(OOH)$[a]	778	738	6
Co^{III}(bleomycin)(OOH)	828	784	8a

[a] L^{Ph} = bis(2-*N*-methylimizadolyl)methylphenylborate; salen = *N*,*N*′-ethylenebis(salicylideneiminato). [b] Center of Fermi doublet.

EPR spectrum of **3** generated in CH_2Cl_2 at −90 °C (Figure 2B) exhibits a rhombic signal with g values at 2.098, 2.011, and 1.980, suggesting an S = 1/2 ground state for **3**. An octet arising from the Co superhyperfine interaction is clearly resolved in the first g component; for the other two, such superhyperfine interactions cannot be readily identified. The computer simulation gives A = 54, 35, 30 MHz for the three principal axis of the g tensor. Compared to **1**, the significantly attenuated A value implies that the unpaired electron mainly localizes in the $O_2^{\bullet-}$ ligand instead of the Co center, demonstrating that **3** consists of a low spin cobalt(III) ion. In fact, analogous EPR spectra with a similar magnitude of Co superhyperfine interactions have been observed for porphyrin cobalt(III)-superoxo complexes,[5a,14] the Co-reconstituted oxyhemoglobin,[5b] and Co-HPCD,[4] all featuring the same electronic structures as **3**. The electron spin echo envelope modulation (ESEEM) measurements at 30 K (Figure S12) detect another

DOI: 10.1021/jacs.6b08642
J. Am. Chem. Soc. 2016, 138, 14186–14189

weak hyperfine interaction, originating from the nitrogen atoms of the $BDPP^{2-}$ ligand. The nuclear quadrupole interaction (NQI) parameters, A_{iso}, A_{aniso}, e^2qQ/h, η are determined to be 1.9, 0.13, 2.55, and 0.3 MHz, respectively, indicating an electron−nucleus interspin distance of 3.5 Å with Euler angles (0°, 17°, 0°) between the NQI and g tensors.

Treatment of **3** with 2,2,6,6-tetramethyl-1-hydroxypiperidine (TEMPOH, BDE_{O-H} = 69.7 kcal/mol)[15] at −90 °C yields a navy blue product, $Co^{III}(BDPP)(OOH)$ (**4**), as demonstrated by the growth of the three new UV−vis absorption bands at 375, 585, and 660 nm (Figure 3). Complex **4** is stable at −80

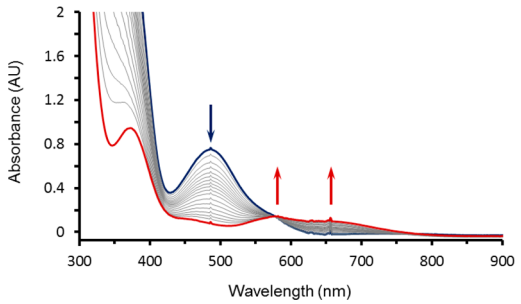

Figure 3. UV−vis spectra derived from conversion of **3** (blue) to **4** (red). Complex **4** was prepared from the reaction of **3** with TEMPOH (2 equiv) added in situ at −90 °C.

°C for weeks and even at 10 °C for 12 hours, making successful crystallization of **4** possible. The crystal structure of **4** reveals that the cobalt center is coordinated by an OOH^- group in addition to the $BDPP^{2-}$ ligand in a pseudo-octahedral coordination environment (Figure 4). All the bond lengths in

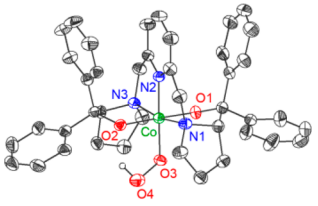

Figure 4. X-ray structure of $Co^{III}(BDPP)(OOH)$ (**4**). ORTEP drawing of **4** is at 50% probability and hydrogen atoms except hydroperoxo hydrogen are omitted for clarity.

the first coordination sphere of **4** are similar to those of **2**, and the determined O−O bond distance of the OOH^- ligand is typical for a metal-bound hydroperoxide reported in the literature (Table S4),[16] indicating that **4** is a cobalt(III)-hydroperoxo complex (Table 1). The Co−OOH moiety exhibits a significantly bent Co−O−O angle of 113.93(14)°. Notably, the Co−O2 bond is elongated by ∼0.038 Å, as compared to Co−O1 bond, which can be traced back to the presence of an intramolecular hydrogen bond between the hydroperoxo proton and O2. In comparison with the ν_{O-O} stretching frequency of **3**, that of **4** shifts to 795 cm^{-1} (λ_{ex} at 457 nm, $\Delta\nu$ = −47 cm^{-1} with $^{18}O_2$, Table 2, Figures S16, S17). The EPR spectra of the reaction solution only show an isotropic feature with a g-value at 2.006, which is attributed to $TEMPO^{\bullet}$, thereby suggesting an S = 0 ground state for **4** as expected for a six-coordinate cobalt(III) complexes. The ^1H NMR spectra of **4** revealed the chemical shift of the hydroperoxo proton at 9.88 ppm, and the signal diminished when D_2O was added (Figure S1). All these observations further confirm the above electronic-structure description for **4**. More importantly, the conversion from **3** to **4** is nearly quantitative in a yield of 90% quantified by the double integration of the radical EPR signal. The yield of $TEMPO^{\bullet}$ decreases as the reaction temperature increases, consistent with the temperature-dependent O_2-binding behavior (vide supra). Taken together, we have presented compelling experimental evidence for stepwise formation of a cobalt(III)-hydroperoxo complex from free O_2 through the superoxo intermediate. The similar HAA reactivity has been found for $Fe^{III}(BDPP)(O_2)$[11] and $[Cr^{III}(14\text{-}TMC)(O_2)(Cl)]^+$.[17] Furthermore, **4** also can be prepared by the reaction of **2** with excess H_2O_2 and NEt_3 (Scheme 1, **2** → **4**, Figure S8), similar to previous reports.[18]

DFT calculations were conducted to compute the geometry and electronic structures of **1**, **3**, and **4**. The calculations at the BP86/TZVP level predict the O−O stretching frequencies at 1141 cm^{-1} for **3** and 820 cm^{-1} for **4**; both values are in a good agreement with those determined by rRaman spectroscopy. As shown in Figure 5, the cobalt(III) ion of **3** resides at the center

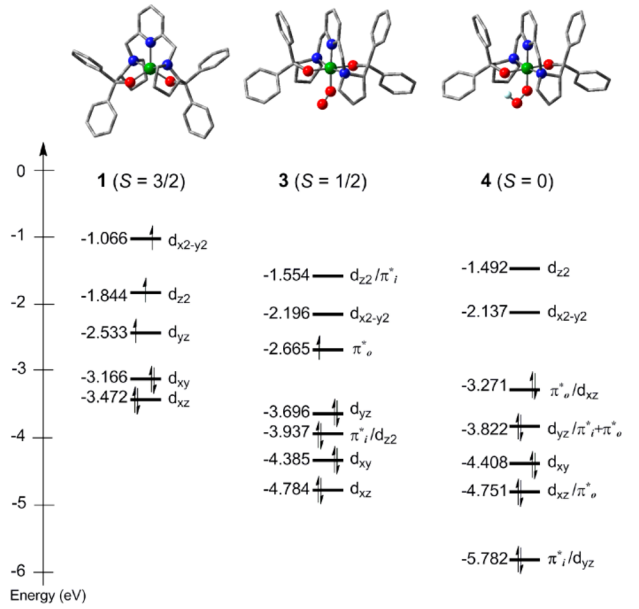

Figure 5. Represented d-manifold splitting patterns and $O_2^{\bullet-}/OOH^-$ π^* orbitals of DFT-optimized **1**, **3**, and **4** where the orbital energies are obtained from their corresponding β-spin orbitals, respectively. The notions i and o of $O_2^{\bullet-}/OOH^-$ π^* orbitals are referred to "in-plane" and "out-of-plane", respectively. The planes for the notations are defined as Co−O−O for **3** and O−O−H for **4**.

of the distorted octahedral coordination environment similar to that observed in the crystal structure of **4**. In addition, the computed average distance (∼3.2 Å) between the center of the superoxo ligand and the coordinated pyrrolidyl nitrogens in **3** (Figure 5) matches that estimated from ESEEM (∼3.5 Å). The optimized structure of **4** reproduces the intramolecular hydrogen bond observed in the X-ray structure, and the hypothetical complex without this interaction (**4′**, Figure S18) is destabilized by ∼6 kcal/mol relative to **4**.

Regarding the d-manifold splitting patterns and the bond formation between Co(BDPP) and $O_2^{\bullet-}/OOH^-$, the corresponding orbital energies of **1**, **3**, and **4** are depicted in Figure 5. Complex **1** possesses a high-spin quartet ground state (S = 3/2) with an electron configuration of $\{d_{xz}^2, d_{xy}^2, d_{yz}^1, d_{z^2}^1, d_{x^2-y^2}^1\}$. Upon O_2 coordination to **1**, the O_2-π^*_i orbital overlaps

DOI: 10.1021/jacs.6b08642
J. Am. Chem. Soc. 2016, 138, 14186−14189

with the Co-d_{z^2} orbital, and hence a pair of bonding (π^*_i/d_{z^2}) and antibonding (d_{z^2}/π^*_i) orbitals (i referred to "in-plane" of Co−O−O for **3**) forms. This bonding interaction dramatically increases the energy gap among the frontier orbitals and facilitates one-electron transfer from Co^{II} to O_2, yielding a $Co^{III}-O_2^{\bullet-}$ adduct with the spin predominantly localized on the $O_2^{\bullet-}$ ligand (~0.96, mostly left in the π^*_o orbital, o referred to "out-of-plane" of Co−O−O for **3**), consistent with the EPR data. In the transformation of **3** to **4**, an additional electron being transferred from the hydrogen atom fills the hole in the π^*_o orbital, thus affording a diamagnetic cobalt(III)-hydroperoxo product.

In summary, we have presented an example that a cobalt(III)-superoxo species is capable of performing a HAA process, by which the structurally characterized nonheme cobalt(III)-hydroperoxo complex is obtained. Interestingly, O_2 binding to five-coordinate cobalt(II) precursor **1** occurs only below −70 °C, yielding **3**, an O_2 adduct. The rRaman and EPR investigations verify that **3** contains a low-spin cobalt(III) center coordinated by a superoxo ligand. Notably, **3** is rather reactive even at −90 °C and can abstract a hydrogen atom from TEMPOH to form metastable cobalt(III)-hydroperoxo **4**. This observation raises an intriguing question whether the C−H cleaving power of the putative Fe-/Co-superoxo intermediate in bleomycin is high enough to break the target C−H bond in ribose, the DNA backbone. A detailed reactivity study of **3** and $Fe^{III}(BDPP)(O_2)$ toward a series of substrate with differential C−H bond strengths, aiming to pinpoint pivotal features that govern the HAA efficiency of metal-superoxo species, is in process.

■ ASSOCIATED CONTENT

Ⓢ Supporting Information

The Supporting Information is available free of charge on the ACS Publications website at DOI: 10.1021/jacs.6b08642.

Experimental procedures, UV−vis, EPR, rRaman spectra, and computational results (PDF)

Crystallographic data of **1**, **2**, **4** (CIF)

■ AUTHOR INFORMATION

Corresponding Authors

*W.-Z.L. wzlee@ntnu.edu.tw
*W.-F.L. wfliaw@mx.nthu.edu.tw
*M.-L.T. mltsai@mail.nsysu.edu.tw
*Y.-W.C. ywchiang@mx.nthu.edu.tw
*S.Y. shengfa.ye@cec.mpg.de

Notes

The authors declare no competing financial interest.

■ ACKNOWLEDGMENTS

This work is supported by the Ministry of Science and Technology of Taiwan (MOST 102-2113-M-003-007-MY3 to W.-Z.L.; MOST 103-2113-M-007-002-MY3 to W.-F.L.; MOST 104-2113-M-110-013-MY2 to M.-L.T.). We also thank National Center for High-performance Computing (NCHC, Taiwan) for computer time and facilities. H.F., F.N., and S.Y. gratefully acknowledge the financial support from the Max-Planck Society. We are indebted to Drs. Eckhard Bill and Maurice van Gastel for fruitful discussions, and to Marion Stapper and Dennis Skerra for rRaman measurements.

■ REFERENCES

(1) (a) Baldwin, J. E.; Bradley, M. *Chem. Rev.* **1990**, *90*, 1079. (b) Roach, P. L.; Clifton, I. J.; Fülöp, V.; Harlos, K.; Barton, G. J.; Hajdu, J.; Andersson, I.; Schofield, C. J.; Baldwin, J. E. *Nature* **1995**, *375*, 700. (c) Roach, P. L.; Clifton, I. J.; Hensgens, C. M. H.; Shibata, N.; Long, A. J.; Strange, R. W.; Hasnain, S. S.; Schofield, C. J.; Baldwin, J. E.; Hajdu, J. *Eur. J. Biochem.* **1996**, *242*, 736. (d) Roach, P. L.; Clifton, I. J.; Hensgens, C. M. H.; Shibata, N.; Schofield, C. J.; Hajdu, J.; Baldwin, J. E. *Nature* **1997**, *387*, 827. (e) Burzlaff, N. I.; Rutledge, P. J.; Clifton, L. J.; Hensgens, C. M. H.; Pickford, M.; Adlington, R. M.; Roach, P. L.; Baldwin, J. E. *Nature* **1999**, *401*, 721. (f) Tamanaha, E.; Zhang, B.; Guo, Y.; Chang, W.-C.; Barr, E. W.; Xing, G.; St. Clair, J.; Ye, S.; Neese, F.; Bollinger, J. M., Jr.; Krebs, C. *J. Am. Chem. Soc.* **2016**, *138*, 8862.

(2) (a) Brown, P. M.; Caradoc-Davies, T. T.; Dickson, J. M. J.; Cooper, G. J. S.; Loomes, K. M.; Baker, E. N. *Proc. Natl. Acad. Sci. U. S. A.* **2006**, *103*, 15032. (b) Xing, G.; Diao, Y.; Hoffart, L. M.; Barr, E. W.; Prabhu, K. S.; Arner, R. J.; Reddy, C. C.; Krebs, C.; Bollinger, J. M., Jr. *Proc. Natl. Acad. Sci. U. S. A.* **2006**, *103*, 6130.

(3) (a) Kovaleva, E. G.; Lipscomb, J. D. *Science* **2007**, *316*, 453. (b) Jeoung, J. H.; Bommer, M.; Lin, T.-Y.; Dobbek, H. *Proc. Natl. Acad. Sci. U. S. A.* **2013**, *110*, 12625. (c) Christian, G. J.; Neese, F.; Ye, S. *Inorg. Chem.* **2016**, *55*, 3853. (d) Christian, G. J.; Ye, S.; Neese, F. *Chem. Sci.* **2012**, *3*, 1600.

(4) Fielding, A. J.; Lipscomb, J. D.; Que, L., Jr. *J. Am. Chem. Soc.* **2012**, *134*, 796.

(5) (a) Smith, T. D.; Pilbrow, J. R. *Coord. Chem. Rev.* **1981**, *39*, 295. (b) Ikeda-Saito, M.; Iizuka, T.; Yamamoto, H.; Kayne, F. J.; Yonetani, T. *J. Biol. Chem.* **1977**, *252*, 4882.

(6) Oddon, F.; Chiba, Y.; Nakazawa, J.; Ohta, T.; Ogura, T.; Hikichi, S. *Angew. Chem., Int. Ed.* **2015**, *54*, 7336.

(7) Anson, C. W.; Ghosh, S.; Hammes-Schiffer, S.; Stahl, S. S. *J. Am. Chem. Soc.* **2016**, *138*, 4186.

(8) (a) Rajani, C.; Kincaid, J. R.; Petering, D. H. *J. Am. Chem. Soc.* **2004**, *126*, 3829. (b) Westre, T. E.; Loeb, K. E.; Zaleski, J. M.; Hedman, B.; Hodgson, K. O.; Solomon, E. I. *J. Am. Chem. Soc.* **1995**, *117*, 1309. (c) Wu, W.; Vanderwall, D. E.; Turner, C. J.; Kozarich, J. W.; Stubbe, J. *J. Am. Chem. Soc.* **1996**, *118*, 1281.

(9) (a) Chen, J.; Stubbe, J. *Nat. Rev. Cancer* **2005**, *5*, 102. (b) Einhorn, L. H. *Proc. Natl. Acad. Sci. U. S. A.* **2002**, *99*, 4592.

(10) (a) Goodwin, K. D.; Lewis, M. A.; Long, E. C.; Georgiadis, M. M. *Proc. Natl. Acad. Sci. U. S. A.* **2008**, *105*, 5052. (b) Burger, R. M. *Chem. Rev.* **1998**, *98*, 1153.

(11) Chiang, C.-W.; Kleespies, S. T.; Stout, H. D.; Meier, K. K.; Li, P.-Y.; Bominaar, E. L.; Que, L., Jr.; Münck, E.; Lee, W.-Z. *J. Am. Chem. Soc.* **2014**, *136*, 10846.

(12) Pfaff, F. F.; Kundu, S.; Risch, M.; Pandian, S.; Heims, F.; Pryjomska-Ray, I.; Haack, P.; Metzinger, R.; Bill, E.; Dau, H.; Comba, P.; Ray, K. *Angew. Chem., Int. Ed.* **2011**, *50*, 1711.

(13) Corcos, A. R.; Villanueva, O.; Walroth, R. C.; Sharma, S. K.; Bacsa, J.; Lancaster, K. M.; MacBeth, C. E.; Berry, J. F. *J. Am. Chem. Soc.* **2016**, *138*, 1796.

(14) Baumgarten, M.; Winscom, C. J.; Lubitz, W. *Appl. Magn. Reson.* **2001**, *20*, 35.

(15) Bordwell, F. G.; Liu, W.-Z. *J. Am. Chem. Soc.* **1996**, *118*, 10819.

(16) Guzei, I. A.; Bakac, A. *Inorg. Chem.* **2001**, *40*, 2390.

(17) Cho, J.; Woo, J.; Nam, W. *J. Am. Chem. Soc.* **2010**, *132*, 5958.

(18) (a) Kim, D.; Cho, J.; Lee, Y.-M.; Sarangi, R.; Nam, W. *Chem. - Eur. J.* **2013**, *19*, 14112. (b) Hikichi, S.; Komatsuzaki, H.; Akita, M.; Moro-oka, Y. *J. Am. Chem. Soc.* **1998**, *120*, 4699.

(19) Hong, S.; Sutherlin, K. D.; Park, J.; Kwon, E.; Siegler, M. A.; Solomon, E. I.; Nam, W. *Nat. Commun.* **2014**, *5*, 5440.

(20) Bajdor, K.; Nakamoto, K.; Kanatomi, H.; Murase, I. *Inorg. Chim. Acta* **1984**, *82*, 207.

(21) Cho, J.; Jeon, S.; Wilson, S. A.; Liu, L. V.; Kang, E. A.; Braymer, J. J.; Lim, M. H.; Hedman, B.; Hodgson, K. O.; Valentine, J. S.; Solomon, E. I.; Nam, W. *Nature* **2011**, *478*, 502.

DOI: 10.1021/jacs.6b08642
J. Am. Chem. Soc. 2016, 138, 14186−14189